

CALORIMETRY OF ACTIVE GALACTIC NUCLEUS JETS: TESTING PLASMA COMPOSITION IN CYGNUS A

M. KINO¹, N. KAWAKATU², AND F. TAKAHARA³

¹ National Astronomical Observatory of Japan, 2-21-1 Osawa, Mitaka, Tokyo 181-8588, Japan
² Graduate School of Pure and Applied Sciences, University of Tsukuba, 305-8571 Tsukuba, Japan
³ Department of Earth and Space Science, Osaka University, 560-0043 Toyonaka, Japan

Received 2011 April 10; accepted 2012 March 19; published 2012 May 10

ABSTRACT

We examine plasma composition of jets in active galactic nuclei through the comparison of the total pressure (P) with partial pressures of electrons and protons in a cocoon. The total pressure is estimated from the analysis of expanding cocoon dynamics. We determine the average kinetic energy per particle for several representative cases of particle energy distribution such as one- and two-temperature thermal plasmas and non-thermal electrons by evaluating the dissipation of the total kinetic energy of the jet into the internal energy of cocoon plasma. The number density of the total electrons/positrons (n_{\pm}) in the cocoon is constrained by using the particle supply from hot spots and the absence of thermal bremsstrahlung emission from radio lobes. By inserting P , n_{\pm} , and the particle energy of each population into the equation of state, the number density (n_p) and pressure (P_p) of protons in the cocoon can be constrained. Applying this method to Cygnus A, we find that (1) electron/positron (e^{\pm}) pairs always dominate in terms of number density, but that (2) either an “ e^{\pm} -supported cocoon (i.e., $P_{\pm} > P_p$)” or a “proton-supported one (i.e., $P_{\pm} < P_p$)” is possible.

Key words: galaxies: individual (Cygnus A) – magnetic fields – radiation mechanisms: non-thermal – radio continuum: galaxies – X-rays: galaxies

1. INTRODUCTION

Elucidating the formation mechanism of relativistic jets in active galactic nuclei (AGNs) is one of the greatest challenges in astrophysics of this century (e.g., Blandford & Znajek 1977; McKinney 2006; Komissarov et al. 2007; McKinney et al. 2012). Plasma composition of jets is a fundamental but difficult issue (see Begelman et al. 1984 for review), because emission timescales of the bulk population such as low-energy electrons/positrons and protons are too long. To examine plasma composition, discrete blobs in blazar jets have been utilized over the years. So far, three approaches have been pursued. The first is based on the synchrotron self-absorption limit combined with total kinetic powers of jets (Reynolds et al. 1996; Hirotani et al. 1999, 2000; Hirotani 2005). The literature indicates the existence of e^{\pm} pair plasma in M 87, 3C 279, and 3C 345. The second is the constraint by the detection of circular polarization. Wardle et al. (1998) and Homan et al. (2009) examined the case of 3C 279 and found that the minimum Lorentz factor of non-thermal electrons/positrons should be much larger than unity for electron–proton (hereafter e/p) content. They rather favored an alternative possibility of dominant e^{\pm} pair content with a small minimum Lorentz factor of non-thermal electrons/positrons (see, however, Ruszkowski & Begelman 2002). The third approach is the constraint from the absence of bulk-Compton emission in flat spectrum radio quasars (Sikora & Madejski 2000; Ghisellini & Tavecchio 2010), and it has been observationally tested for PKS 1510–089 and SWIFT J0746.3+2548 (Kataoka et al. 2008; Watanabe et al. 2009). The same approach has also been applied to the kiloparsec-scale knots in PKS 0637–752 (Georganopoulos et al. 2005; Uchiyama et al. 2005; Mehta et al. 2009). They claim that jets contain more e^+e^- pairs than protons, but that jets are dynamically dominated by protons. However, it should be noted that the estimate of a total kinetic power L_j of each blob is difficult because of the existence of invisible components such as low-energy electrons/positrons and protons. Therefore, the

assumption of constant L_j was made, and the L_j are inferred from non-thermal emissions. Since plasma composition is sensitive to L_j , a better estimate of L_j is essential. Regarding the estimate of L_j , it is essential to take into account the thermal component (e.g., Kino & Takahara 2008).

Cocoons associated with Fanaroff-Riley I and II (FR I and FR II) radio galaxies are also known to be good tools for exploring plasma composition. In contrast to blobs in blazars, investigations using cocoon dynamics allow us to better estimate the energy injection into the cocoon. The total pressure P can be estimated with fewer uncertainties based on the dynamic interaction between jets and the intracluster medium (ICM), and P involves the contributions of invisible components (e.g., Rawlings & Saunders 1991; Fabian et al. 2002). For FR I radio galaxies, many authors have discussed the ratio of P to that of non-thermal electrons ($P_{\text{NT}}^{\text{NT}}$) for various sources based on observed non-thermal emissions (e.g., Dunn et al. 2005; Croston et al. 2005; Rafferty et al. 2006; De Young 2006; Bîrzan et al. 2008). First of all, we should emphasize that these studies indicate that the total pressure P tends to be greater than that of non-thermal electrons, i.e., $P > P_{\text{NT}}^{\text{NT}}$ (e.g., Bîrzan et al. 2008). This means that the finite pressure of low-energy electrons/positrons and/or protons is required in these sources. The derived $P/P_{\text{NT}}^{\text{NT}}$ values in the previous work extend over a wide range from the order of unity to thousands (e.g., Bîrzan et al. 2008; Cavagnolo et al. 2010). For FR I sources, however, an entrainment process of surrounding medium via the jet boundary layer could work (e.g., De Young 1993; Bicknell 1984; Rossi et al. 2008), and the process makes jets heavier. Therefore, jets in FR I sources could undergo severe proton loading during their propagations, and this could cause the large scatter of $P/P_{\text{NT}}^{\text{NT}}$.

In this work, we focus on FR II radio galaxies (Figure 1) from the viewpoint of the important advantage they represent. Contrary to FR I sources, we know from relativistic hydrodynamic simulations that no significant entrainment appears for FR II sources (Scheck et al. 2002; Mizuta et al. 2004). Therefore, a plasma composition test for FR II radio galaxies would allow

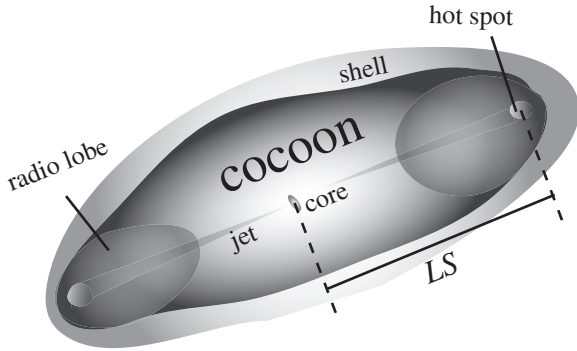


Figure 1. Schematic of a powerful FR II radio galaxy. A pair of jets are ejected from the core, and they are decelerated via strong shocks. The shocks are identified as the hot spots and the remnant of decelerated jets envelop the overall jet system; this is identified as a cocoon. Part of the cocoon is normally observed as radio lobes. The cocoon head and the hot spots advance at a speed v_{hs} . Swept-up ambient matter becomes a shell and surrounds the cocoon. The projected linear size is denoted as LS in this work.

us to give better constraints on plasma composition in AGN jets without an entrainment effect. Regarding an observational indication of a difference between total and non-thermal pressures in FR II radio galaxies, Ito et al. (2008, hereafter I08) recently examined the following sources: Cygnus A, 3C 223, 3C 284, and 3C 219. In I08, they show that the energy density of the total plasma is greater than the energy density of non-thermal electrons by a factor of 4–310 in the case of a minimum-energy condition (e.g., Miley 1980; Kellermann & Pauliny-Toth 1981). This implies that the minimum-energy condition is violated, particle energy is dominant, and low-energy electrons/positrons and/or protons (i.e., cosmic rays) are required to explain the total P in these FR II sources.

In Section 2, we describe the basic idea and assumptions of our method. In Section 3, we briefly explain the dynamic determination of the total pressure in the cocoon. In Section 4, we express P as a function of the number density ratio of protons to electrons. In Section 5, we explain details of the plasma composition test, which is applied to Cygnus A in Section 6. Summary and discussions are given in Section 7.

2. METHOD AND PROBLEM SETTING

Here, we describe the basic idea and assumptions of our method. In this work, the number densities of protons (n_p), positrons (n_+), and electrons (n_-) are related using the parameter η as follows:

$$\begin{aligned} n_p &\equiv \eta n_- \\ n_+ &= (1 - \eta)n_- \quad (0 \leq \eta \leq 1), \end{aligned} \quad (1)$$

where the latter relation is derived from the charge neutrality condition. The case of $\eta = 0$ corresponds to pure e^\pm plasma, while $\eta = 1$ corresponds to the pure e/p plasma. We denote that $n_p = n_p^T + n_p^{NT}$, $n_- = n_-^T + n_-^{NT}$, $n_+ = n_+^T + n_+^{NT}$, and $n_\pm = n_- + n_+$, where n_\pm is the sum of the total number densities of electrons and positrons. Hereafter, superscripts T and NT represent thermal and non-thermal components, respectively. The distinction between thermal and non-thermal particles may not be trivial for relativistic plasmas. In this paper, we relate the thermal component to Maxwellian-like distribution characterized by the temperature, while we relate the non-thermal one to particles following a power-law distribution characterized by the power-law index and minimum and maximum energies as

detailed below. Since we focus on relativistic plasmas in the present work, the thermal component correspondingly has a relativistic temperature. Hence, one should be cautious since most of observational papers refer the thermal component to non-relativistic plasmas (e.g., Garrington & Conway 1991).

The allocation of partial pressure of each plasma population is the central concern of this paper. In general, P is decomposed to

$$\begin{aligned} P &= P_- + P_+ + P_p + P_B \\ &= P_-^T + P_+^T + P_-^{NT} + P_+^{NT} + P_p^T + P_p^{NT} + P_B, \end{aligned} \quad (2)$$

where P_-^T , P_+^T , P_p^T , P_-^{NT} , P_+^{NT} , P_p^{NT} , and P_B are the partial pressures of thermal (T) electrons, thermal positrons, thermal protons, non-thermal (NT) electrons, non-thermal positrons, non-thermal protons, and the magnetic pressure, respectively. We also define $P_\pm = P_- + P_+$ as the sum of the total pressures of electrons and positrons. Throughout this work, we do not include the magnetic pressure because it is sub-dominant in P . Isobe et al. (2005) summarize the energy density of energetic electrons as typically being 10 times larger than that of magnetic fields in various radio lobes (e.g., Isobe et al. 2002; Tashiro et al. 1998, 2009; Hardcastle & Croston 2010), and it also holds in Cygnus A (Yaji et al. 2010).

2.1. Basic Idea of the Method

The essence of our method is as follows: First, the total pressure in the cocoon (P) is determined through dynamic considerations following I08, where they obtained P via the comparison of the expanding cocoon model with radio observations. Second, average energy per particle in the cocoon is evaluated. It is essential that our formulation is based on the basic conservation laws of mass, momentum, and energy in the cocoon. Since it depends on coupling of protons to the electrons/positrons, we examine several representative cases with different equations of state. Third, n_- can be partially constrained using the absence of thermal bremsstrahlung emission from the cocoon and the supply rate of electrons from the hot spots. Finally, n_p and P_p can be obtained by inserting the obtained quantities into the equation of state (EOS).

2.2. On Particle Distribution Functions

Since observational data at low frequencies below GHz are quite limited, it is hard to explore the properties of low-energy electrons (including positrons). Bearing this difficulty in mind, we pick up plausible cases of electron distribution function. As in the canonical case referred to as case (a), we consider two-temperature thermal plasmas, where protons and electrons have different temperatures and contributions of non-thermal components to the total pressure are negligible. As an alternative, we also examine case (b), in which protons and electrons take the same temperature without non-thermal components.

We further explore two cases, (c) and (d), in which the non-thermal population makes a dominant contribution to the total pressure with negligible pressure from the thermal population. For the non-thermal population, we assume the power-law distribution functions

$$\begin{aligned} n_-^{NT}(\gamma_-) &\propto \gamma_-^{-s_e} (\gamma_{-,min} \leq \gamma_- \leq \gamma_{-,max}) \text{ and} \\ n_p^{NT}(\gamma_p) &\propto \gamma_p^{-s_p} (\gamma_{p,min} \leq \gamma_p \leq \gamma_{p,max}) \end{aligned} \quad (3)$$

for case (c) with $s_p = s_e > 2$. Observations of the spectral index in the radio lobe of Cygnus A suggest $s_e > 2$ (e.g., Carilli et al. 1991; Yajii et al. 2010).

Last, we set case (d), in which the number spectrum of non-thermal electrons is given by a broken power law:

$$n_{-}^{\text{NT}}(\gamma_{-}) \propto \begin{cases} \gamma_{-}^{-s_{e,1}} & (\gamma_{-, \text{min}} \leq \gamma_{-} \leq \gamma_{-, \text{crit}}), \\ \gamma_{-, \text{crit}}^{s_{e,2}-s_1} \gamma_{-}^{-s_{e,2}} & (\gamma_{-, \text{crit}} \leq \gamma_{-} \leq \gamma_{-, \text{max}}), \end{cases}$$

$$n_{p}^{\text{NT}}(\gamma_p) \propto \gamma_p^{-s_p} (\gamma_{p, \text{min}} \leq \gamma_p \leq \gamma_{p, \text{max}}), \quad (4)$$

where $s_{e,1} < 2$ and $s_p > 2$ are satisfied. This model is based on Stawarz et al. (2007), who suggested that observed spectra at the jet termination shock (hot spot) of FR II jets (Cygnus A) can be explained by the break at non-thermal electron energy (hereafter $\gamma_{\pm, \text{crit}}$). This type of spectra may be due to the absorption of electromagnetic waves emitted at the harmonics of cyclotron frequency of cold protons, as discussed by Hoshino et al. (1992) and Amato & Arons (2006). Some observations for other FR II sources could also be compatible with this picture (e.g., Perlman et al. 2010 for 3C445).

For cases (c) and (d), the minimum energy of non-thermal electrons/positrons ($\gamma_{\pm, \text{min}} m_e c^2$) and protons ($\gamma_{p, \text{min}} m_p c^2$) are generally assumed as

$$\gamma_{\pm, \text{min}} \approx \gamma_{p, \text{min}} \approx \Gamma_j, \quad (5)$$

which is expected when protons and electrons/positrons are separately heated and accelerated at termination shocks. On the other hand, the values of the maximum energy of non-thermal pairs ($\gamma_{\pm, \text{max}} m_e c^2$) and protons ($\gamma_{p, \text{max}} m_p c^2$) are largely uncertain. While $\gamma_{\pm, \text{max}} m_e c^2$ may be significantly affected by radiative coolings, $\gamma_{p, \text{max}} m_p c^2$ may reach the range of highest energy cosmic rays (e.g., Takahara 1990; Rachen & Biermann 1993). It is reasonable to suppose that $\gamma_{\pm, \text{max}} \gg \gamma_{\pm, \text{min}}$ and $\gamma_{p, \text{max}} \gg \gamma_{p, \text{min}}$.

3. TOTAL PRESSURE P

In this section, we briefly describe the basic idea of estimating the total pressure P . In Figure 1 we show a schematic of the interaction of the jet and ICM. Heating and acceleration processes work at hot spots and those particles are injected into cocoons. The cocoon model was proposed by Begelman & Cioffi (1989), in which the dissipated energy of jet bulk motion is the origin of the total pressure of cocoon, and a cocoon of FR IIs is expected to be overpressured against ICM pressure (P_{ICM}) with a significant sideways expansion. Therefore, the assumption of $P = P_{\text{ICM}}$ is not valid. We have proposed a method of dynamic constraint of P by comparison of the cocoon model with the actually observed morphology of the cocoons (Kino & Kawakatu 2005; I08), and this method is applied to various radio lobes (e.g., Machalski et al. 2010). We use this model in the present work. The reliability of the expanding cocoon model is well examined in Kawakatu & Kino (2006). The results of relativistic hydrodynamic simulations of Scheck et al. (2002) and Perucho & Martí (2007) support the above analytic model. The mass and energy injections from the jet into the cocoon, which govern the cocoon pressure P and mass density ρ averaged by the source age (t_{age}), are written as

$$\frac{\hat{\gamma}}{\hat{\gamma} - 1} \frac{PV}{t_{\text{age}}} = 2T_j^{01} A_j \equiv 2L_j, \quad T_j^{01} = \rho_j c^2 \Gamma_j^2 v_j, \quad (6)$$

$$\frac{\rho V}{t_{\text{age}}} = 2J_j A_j, \quad J_j = \rho_j \Gamma_j v_j, \quad (7)$$

where $\hat{\gamma}$, V , A_j , T_j^{01} , J_j , ρ_j , and Γ_j are the adiabatic index of the plasma in the cocoon, the volume of the cocoon, the cross-sectional area, the total energy flux, the rest mass flux, the rest mass density, and the bulk Lorentz factor of the jet, respectively. The term V is evaluated as $V = 2(\pi/3)\mathcal{R}^2\text{LS}^3$, where LS and \mathcal{R} are the linear size of the cocoon along the jet axis and the aspect ratio of the cocoon, respectively. Here, we denote physical quantities of the jet with the subscript j . Throughout this work, we focus on a relativistic jet. Correspondingly, the shocked plasma has relativistic energy; thus, we take $\hat{\gamma} = 4/3$. The PdV work done by the cocoon against ICM is taken into account in the energy equation (6) following I08. For a given ρ_{ICM} , we can dynamically estimate total pressure P by measuring LS , \mathcal{R} , and the head cross-sectional area of the cocoon. Here, the relations of $\text{LS} = \beta_{\text{hs}} c t_{\text{age}}$ and $\mathcal{R} \equiv l_c / \text{LS} < 1$ hold, where l_c and $\beta_{\text{hs}} c$ are the lateral size of the cocoon and the advance velocity of the hot spot, respectively. Since \mathcal{R} and β_{hs} have some uncertainties, actual P is bounded by maximum and minimum values

$$P_{\text{min}} \leq P \leq P_{\text{max}}. \quad (8)$$

Thus, we can obtain the total pressure of cocoon P , which includes the partial pressures of non-radiating particles. The estimate of P has actually been done by I08 for some FR II sources, and we adopt P values in I08 in this work.

4. PRESSURE AS A FUNCTION OF η

In this section, we express P as a sum of the partial pressures and represent it as a function of η for respective cases.

4.1. Case (a)

First, we examine the canonical case of two-temperature thermal plasma. Here, we assume that $P_{-}^{\text{NT}} = P_{+}^{\text{NT}} = P_p^{\text{NT}} = 0$ and $n_{-}^{\text{NT}} = n_{+}^{\text{NT}} = n_p^{\text{NT}} = 0$. The EOS in the cocoon filled with relativistic plasma is given by

$$P \approx P_{\pm}^{\text{T}} + P_p^{\text{T}} = (n_{-}^{\text{T}} + n_{+}^{\text{T}})kT_{\pm} + n_p^{\text{T}}kT_p, \quad (9)$$

where T_{\pm} and T_p are the electron/positron temperature and proton temperature, respectively. Hereafter, we adopt $T_{\pm} = T_{-} = T_{+}$, where T_{-} and T_{+} are the temperatures of the electrons and positrons, respectively. Following Kino et al. (2007), we can obtain T_{\pm} and T_p from Equations (6), (7), and (9):

$$kT_{\pm} = \frac{\Gamma_j m_e c^2}{4}, \quad kT_p = \frac{\Gamma_j m_p c^2}{4}, \quad (10)$$

which are typically given by $kT_{\pm} = 1.3(\Gamma_j/10)$ MeV and $kT_p = 2.3(\Gamma_j/10)$ GeV. Here, we assume the limit of inefficient e/p -coupling, i.e., protons and electrons are separately thermalized so that $kT_{\pm} = (m_e/m_p)kT_p$, since plasma number densities in large scale jets are conservatively expected to be too diluted to achieve efficient e/p -coupling (e.g., Kino et al. 2007 and references therein). The emission timescale is so long that radiative cooling is negligible. It is worth noting that the

geometric factors in Equations (6) and (7) are completely canceled out and kT_{\pm} and kT_p are governed only by Γ_j .

Inserting Equation (10) into Equation (9), we rewrite the total pressure in the cocoon P as

$$P(\eta) = 2.05 \times 10^{-6} n_{\pm}^T \left[(2 - \eta) + \eta \frac{m_p}{m_e} \right] \left(\frac{\Gamma_j}{10} \right) \text{ erg cm}^{-3}, \quad (11)$$

where the first and second terms in the square brackets correspond to the partial pressure of pairs and protons, respectively.

4.2. Case (b)

As an opposite extreme to case (a), here we consider the case of one-temperature plasma. In this example, some of the proton energy is somehow transferred to electrons/positrons to achieve an efficient e/p -coupling. Then, hotter electrons/positrons and colder protons are produced. From the condition $kT_{\pm} = kT_p$, and Equations (6) and (7), we obtain

$$kT_{\pm} = kT_p = \frac{\Gamma_j m_e c^2}{8} \left[(2 - \eta) + \eta \frac{m_p}{m_e} \right]. \quad (12)$$

In this case, each population (i.e., $p/e^-/e^+$) has the same kinetic energy. The total pressure is given by Equation (11), the same as case (a). The essential difference from case (a) is that kT_{\pm} in case (b) is much higher than that in case (a).

4.3. Case (c)

For comparison with the canonical case (a), we examine case (c), in which the cocoon pressure is dominated by non-thermal particles. Case (c) concerns a situation in which the spectral indices of non-thermal particle energy distributions satisfy $s_p = s_e > 2$ as some theoretical work on relativistic shocks suggests (e.g., Bednarz & Ostrowski 1998; Kirk et al. 2000; Achterberg et al. 2001; Spitkovsky 2008; Sironi & Spitkovsky 2011) and as the radio lobes of Cygnus A show $s_e > 2$ (e.g., Carilli et al. 1991; Yaji et al. 2010). In this case, electrons and protons with the lowest energies are the main carriers of energy. Then, the evaluation of partial pressures of non-thermal plasma is basically the same as in case (a) when we replace kT_{\pm} with $\gamma_{\pm, \min} m_e c^2$ and kT_p with $\gamma_{p, \min} m_p c^2$. Then, P is given by

$$P(\eta) = \frac{\Gamma_j n_{\pm}^{\text{NT}} m_e c^2}{3} \frac{s_e - 1}{s_e - 2} \left[(2 - \eta) + \eta \frac{m_p}{m_e} \right]. \quad (13)$$

From this, it is clear that we can appropriately evaluate η for case (c) by replacing n_{\pm}^T with n_{\pm}^{NT} in the same way as is done in case (a).

4.4. Case (d)

Here, we examine the pressure of non-thermal electrons when they follow a broken power-law spectrum (Equation (4)). Stawarz et al. (2007) indicated $\gamma_{\pm, \text{crit}} \sim m_p/m_e$ for the hot spots in Cygnus A. The energy of the electron component is governed by those with break energy, while the number is dominated by those with lowest energies. Since $s_p > 2$ is satisfied, lowest-energy protons carry most of the energy. Therefore, the total pressure P is expressed as

$$P(\eta) = \frac{\Gamma_j n_{\pm}^{\text{NT}} m_e c^2}{3} \left[\frac{s_{e,1} - 1}{-s_{e,1} + 2} A_{\pm} (2 - \eta) + \frac{s_p - 1}{s_p - 2} \eta \frac{m_p}{m_e} \right], \quad (14)$$

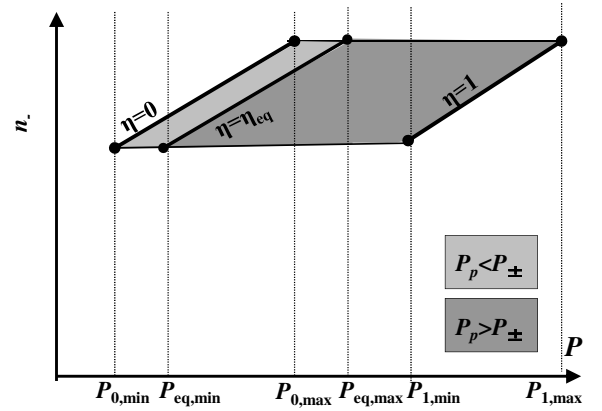


Figure 2. Schematic diagram of the allowed region of $n_{-}(P)$ plotted vs. the cocoon pressure P for given Γ_j . They are limited by $n_{-, \min} \leq n_{-} \leq n_{-, \max}$ and $0 \leq \eta \leq 1$. The region of the e^{\pm} -supported cocoon ($P_{\pm} > P_p$) is colored in light gray, while the region of the proton-supported cocoon ($P_p > P_{\pm}$) is colored in dark gray.

where $A_{\pm} = (\gamma_{\pm, \text{crit}}/\gamma_{\pm, \min})^{-s_{e,1}+2}$. Thus, η can be evaluated when we replace n_{\pm}^T with n_{\pm}^{NT} and include factor A_{\pm} .

5. TESTING PLASMA COMPOSITION

We explain the method for constraining plasma composition of AGN jets for thermal plasma cases (a) and (b) in 5.1, 5.2, and 5.3. The application to non-thermal plasma cases (c) and (d) can be readily understood and is explained in 5.4.

5.1. Characteristic Pressures

First, we define characteristic pressures that divide the number-density/pressure plane into several regions as shown in Figure 2. As a preparation, here we define η_{eq} as follows:

$$\eta_{\text{eq}} \equiv \frac{2}{m_p/m_e - 1} = 1.1 \times 10^{-3} \quad (P_{\pm} = P_p). \quad (15)$$

The partial pressure of proton-associated electrons is implicitly neglected since it is subdominant in the case of inefficient e/p -coupling. The line with $n_{-} = 1 \times 10^3 n_p$ divides the pair-supported and proton-supported cocoons in the limit of inefficient e/p -coupling plasma. By definition, the cocoon with $\eta > \eta_{\text{eq}}$ is proton-supported (dark gray region in Figure 2), while the cocoon with $\eta < \eta_{\text{eq}}$ is pair-supported (light gray region in Figure 2). When n_{-} is bounded by $n_{-, \min}$ and $n_{-, \max}$ as argued in the next subsection, the allowed region of n_{-} is segmented by some characteristic pressures by the characteristic values of n_{-} and η , i.e., $n_{-, \min}$, $n_{-, \max}$, $\eta = 0$, $\eta = \eta_{\text{eq}}$, and $\eta = 1$. Here, we define six characteristic pressures as follows:

$$\begin{aligned} P(\eta = 0; n_{-} = n_{-, \min}) &\equiv P_{0, \min}, \\ P(\eta = \eta_{\text{eq}}; n_{-} = n_{-, \min}) &\equiv P_{\text{eq}, \min}, \\ P(\eta = 0; n_{-} = n_{-, \max}) &\equiv P_{0, \max}, \\ P(\eta = \eta_{\text{eq}}; n_{-} = n_{-, \max}) &\equiv P_{\text{eq}, \max}, \\ P(\eta = 1; n_{-} = n_{-, \min}) &\equiv P_{1, \min}, \\ P(\eta = 1; n_{-} = n_{-, \max}) &\equiv P_{1, \max}. \end{aligned} \quad (16)$$

Then, by definition, we have the following relations:

$$\begin{aligned} P_{0, \min} : P_{\text{eq}, \min} : P_{0, \max} : P_{\text{eq}, \max} : P_{1, \min} : P_{1, \max} \\ = 1 : 2 : \frac{n_{-, \max}}{n_{-, \min}} : 2 \frac{n_{-, \max}}{n_{-, \min}} : \frac{m_p}{m_e} : \frac{m_p}{m_e} \frac{n_{-, \max}}{n_{-, \min}}, \end{aligned} \quad (17)$$

where we approximate $2 - \eta_{\text{eq}} \approx 2$. To evaluate these pressures, we estimate $n_{-, \text{min}}$ and $n_{-, \text{max}}$ in the next subsection.

5.2. Estimation of n_-

Here, we constrain the number density of electrons in the cocoon (n_-). We denote the lower and upper limits of n_- as $n_{-, \text{min}}$ and $n_{-, \text{max}}$, respectively. The values of $n_{-, \text{min}}$ and $n_{-, \text{max}}$ are independently constrained; we show them below.

5.2.1. Lower Limit of n_-

Here, we estimate the lower limit of n_- and examine the case in which the number density of thermal electrons is greater than that of non-thermal electrons $n_-^{\text{T}} \geq n_-^{\text{NT}}$, since non-thermal electrons are partially injected from the background thermal electrons. (Later, the extreme cases of $n_-^{\text{T}} \leq n_-^{\text{NT}}$ will also be discussed, as they are identical to cases (c) and (d)). Since the shocked plasma at hot spots expands sideways and is injected into the cocoon, we can estimate n_-^{T} by using $n_{\text{hs}}^{\text{NT}}$, where $n_{\text{hs}}^{\text{NT}}$ is the number density of non-thermal electrons in a hot spot. We stress that $n_{\text{hs}}^{\text{NT}}$ is well constrained by observed non-thermal emissions of hot spots for FR II sources (see, e.g., Harris & Krawczynski 2006 for review). By connecting the number density from the jet to the cocoon based on Equation (7) and shock conditions along the jet axis shown in Kino & Takahara (2004, hereafter KT04), we obtain

$$n_{-, \text{min}} = \frac{n_{\text{hs}}^{\text{NT}} A_j L S}{2V \beta_{\text{hs}}}. \quad (18)$$

In general, number density of non-thermal electrons with power-law distribution $n_{\text{hs}}^{\text{NT}} \propto \int_{\gamma_{\text{hs}, \text{min}}}^{\gamma_{\text{hs}, \text{max}}} \gamma_{\text{hs}}^{-s_{\text{hs}}} d\gamma_{\text{hs}}$ can be given by

$$n_{\text{hs}}^{\text{NT}} \propto \gamma_{\text{hs}, \text{min}}^{-s_{\text{hs}}+1}. \quad (19)$$

We assume the standard value of $s_{\text{hs}} \approx 2$ and $\gamma_{\text{hs}, \text{min}} \approx \Gamma_j$.

5.2.2. Upper Limit of n_-

The upper limit of n_- can be constrained by the absence of thermal bremsstrahlung from hot electrons in the cocoon/lobes viewed in X-ray observations (Wilson et al. 2000, 2006). The observed X-ray emissions associated with radio lobes are non-thermal emissions, and there is no evidence of thermal X-ray emission from cocoons/lobes (see Harris & Krawczynski 2006 for review). From this, we can safely use the condition of $L_{\text{X, obs}} > L_{\text{brem}}(n_-^{\text{T}}, T_{\pm})$, where $L_{\text{brem}}/V = \alpha_f r_e^2 m_e c^3 (n_-^{\text{T}})^2 F_{\pm}(\Theta_{\pm}) \text{ erg s}^{-1} \text{ cm}^{-3}$, $F_{\pm}(\Theta_{\pm}) = 48\Theta_{\pm}(\ln 1.1\Theta_{\pm} + 5/4)$, and $\Theta_{\pm} = kT_{\pm}/m_e c^2$, for bremsstrahlung at relativistic temperature (Equation (22) in Svensson 1982), and α_f and r_e are the fine structure constant and the classical electron radius, respectively. From this, we obtain the maximum n_- as follows:

$$n_{-, \text{max}} = \left(\frac{L_{\text{brem}}}{V \alpha_f r_e^2 m_e c^3 F_{\pm}(\Theta_{\pm})} \right)^{1/2}. \quad (20)$$

It is worth commenting on the availability of constraining the upper limit of n_- by the analysis of the internal depolarization of the radio lobes. Relativistic plasma makes a smaller contribution to Faraday rotations since electron inertia increases for the relativistic regime, and it suppresses rotations of the polarization angle (e.g., Ichimaru 1973; Melrose 1997; Quataert & Gruzinov 2000; Huang & Shcherbakov 2011). Therefore, it is not effective to use the constraint by rotation measure (RM) in the present work.

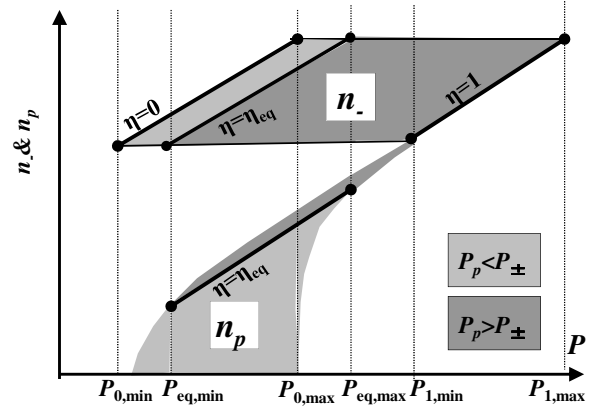


Figure 3. Same as Figure 2 but including the allowed region of n_p . When $\eta = 1$, $n_- = n_p$ holds by definition. When $\eta < 1$, a positron mixture is required by the charge neutrality condition of $n_- = n_p + n_+$. The plane is divided into five regions by characteristic pressures. The actual allowed region is further limited within $P_{\text{min}} \leq P \leq P_{\text{max}}$ by the consideration of cocoon calorimetry.

5.3. Estimation of n_p

Once n_- is estimated, the proton number density n_p can be determined as

$$n_p = \eta n_-, \quad (21)$$

by definition. Here, of course, the conditions of $0 \leq \eta \leq 1$ and $n_{-, \text{min}} \leq n_- \leq n_{-, \text{max}}$ are imposed. In Figure 3, the allowed region of n_p is added to that of n_- shown in Figure 2. In the same way as in Figure 2, the plane is divided into five regions.

Finally, the allowed regions of n_p and n_- can be obtained by adjoining the range of P . The allowed regions drawn in Figure 3 are bound by Equation (8). Thus, we can obtain the definitive allowed regions of n_p and n_- .

5.4. Application to Cases (c) and (d)

In Sections 5.1, 5.2, and 5.3, we considered physical quantities associated with thermal plasma in cases (a) and (b). But those can also be applied to non-thermal plasma by the proper replacements of number densities and average energies of particles. With regard to average energies, we have already explained the replacements in the previous section. As for $n_{-, \text{min}}$, the estimate shown in Section 5.2.1 can be applied for both thermal and non-thermal plasmas. As for $n_{-, \text{max}}$, the estimate shown in Section 5.2.2 can be applied only for thermal plasma. Therefore, we do not use $n_{-, \text{max}}$ for the cases (c) and (d). Thus, we can properly estimate η for cases (c) and (d).

6. APPLICATION TO CYGNUS A

Here, we apply the above method to Cygnus A ($z = 0.0562$), which is one of the best-studied FR II radio galaxies (e.g., Carilli & Barthel 1996; Steenbrugge et al. 2008, 2010; Yaji et al. 2010). The physical quantities of Cygnus A have been well constrained by previous works. To constrain the real values of P and n_- , we carefully evaluate \mathcal{R} , β_{hs} , and Γ_j . The term \mathcal{R} has an effect on n_- via a cocoon volume V . The term Γ_j is directly proportional to P . The term β_{hs} controls the source age t_{age} , which governs the injection rates of mass and energy into the cocoon. These are summarized in Section 6.1. The resultant allowed region of n_- and n_p is summarized in Section 6.2.

6.1. Viable Ranges of Physical Quantities

We show adopted conditions of the model parameters for deriving the above results. We fix the cross section area of the jet as $A_j = \pi R_{\text{hs}}^2 = \pi(2 \text{ kpc})^2$ (Wilson et al. 2000) and the number density of ICM just ahead of the hot spot as $n_{\text{ICM}} = 0.5 \times 10^{-2} \text{ cm}^{-3}$ (the shell No. 6 in Table 5 in Smith et al. 2002).

1. *Cocoon morphology* \mathcal{R} . From images of the Cygnus A cocoon, we can directly constrain \mathcal{R} . The upper limit $\mathcal{R} \approx 0.5$ is determined by the *Chandra* X-ray image (Wilson et al. 2000, 2006; Yaji et al. 2010). The lower limit $\mathcal{R} \approx 0.25$ is directly measured by the 330 MHz Very Large Array (VLA) image (see also Carilli et al. 1991; Lazio et al. 2006). Therefore, we set

$$0.25 \leq \mathcal{R} \leq 0.5$$

in the present work.

2. *Cocoon head velocity* β_{hs} . Cocoon head velocity, which equals the hot spot advance velocity (β_{hs}), is well constrained by the synchrotron aging method. The estimated β_{hs} has some uncertainty due to the uncertainty of magnetic field strength in the cocoon. From the result of synchrotron aging diagnosis in Carilli et al. (1991), we adopt the allowed range of β_{hs} as

$$0.01 \leq \beta_{\text{hs}} \leq 0.06.$$

We emphasize that sufficiently large uncertainty is taken into account here. The adopted value of β_{hs} is quite typical for hot spots in FR II radio galaxies (e.g., Scheuer 1995).

3. *Lorentz factor of the jet* Γ_j . It is difficult to determine the true velocity of the jet. At least we may say that apparent velocity of blobs obtained by very long baseline interferometry (VLBI) observations shows a minimum velocity of underlying flow. A fast apparent motion of a blob at the jet base (0.56 ± 0.28) c has been reported by VLBI observations (Bach et al. 2003). Furthermore, suggestions of superluminal motion have been made (Krichbaum et al. 1998; Bach et al. 2002) although they have not been clearly confirmed. On VLA scale, a clear asymmetry in brightness distribution of a kiloparsec-scale jet due to a relativistic motion is seen (Perley et al. 1984). Therefore, overall radio observations seem to indicate relativistic motion. Bearing this in mind, we assume that the jet is relativistic and the four-velocity of the jet $\Gamma_j \beta_j$ is set as

$$1 \leq \Gamma_j \beta_j \leq 30.$$

Here, the upper limit is assumed to be $\Gamma_j \approx 30$ based on the statistical study of radio jets of MOJAVE sources (Lister et al. 2001, 2009; Kellermann et al. 2004).

4. *Cocoon pressure* P . Using the value of $V = 1 \times 10^{70} \mathcal{R}^2 \text{ cm}^3$, we can estimate the total pressure P as

$$8 \times 10^{-11} \text{ erg cm}^{-3} \leq P \leq 4 \times 10^{-9} \text{ erg cm}^{-3}. \quad (22)$$

The lower limit equals the ICM pressure $8 \times 10^{-11} \text{ erg cm}^{-3}$ measured by Arnaud et al. (1984) to satisfy the overpressured cocoon condition. Although the upper limit of P is basically adopted from I08, the value $4 \times 10^{-9} \text{ erg cm}^{-3}$ is four times larger than the original estimate in I08. This is due to the change in minimum value of \mathcal{R} from 0.5 to 0.25 based on

VLA's 0.3 GHz image. It should be stressed that our adoption of the allowed range of P is sufficiently wide compared with all of the previous work (see, e.g., Carilli et al. 1998 for review). Note that Yaji et al. (2010) estimate that P_{NT} in the radio lobes is $P_{\text{NT}} \approx (1-2) \times 10^{-9} \text{ erg cm}^{-3}$ for $\gamma_{\pm} \approx 1$, which causes $P_{\text{NT}} > P_{\text{min}}$. So, if P completely equals the radio lobe pressure, then the range $P_{\text{min}} \leq P < P_{\text{NT}}$ is excluded and the allowed P range becomes narrower. The allowed example with $P_{\text{min}} \leq P_{\text{NT}} \leq P \leq P_{\text{max}}$ is involved in cases (c) and (d).

5. *Non-thermal electron number density* $n_{\text{hs}}^{\text{NT}}$. The lower limit $n_{\text{hs},\text{min}}^{\text{NT}}$ largely depends on $n_{\text{hs}}^{\text{NT}}$. For $s_{\text{hs}} = 2$, the number density of non-thermal electrons in the hot spot can be obtained from

$$n_{\text{hs}}^{\text{NT}} \approx 1 \times 10^{-3} \left(\frac{\gamma_{\text{hs},\text{min}}}{10} \right)^{-1} \text{ cm}^{-3}, \quad (23)$$

via detailed comparisons of the SSC model with the observed broadband spectrum (Wilson et al. 2000; KT04; Stawarz et al. 2007) where $\gamma_{\text{hs},\text{min}} \approx \Gamma_j$. We stress that these three independent papers derive similar values of $n_{\text{hs}}^{\text{NT}}$, although Stawarz et al. (2007) adopt the different electron-distribution function shown in Equation (4). Furthermore, we note the importance of low-frequency radio spectra since it affects the estimate of $n_{\text{hs}}^{\text{NT}}$. Regarding low-frequency radio observation, we briefly comment on the work of Lazio et al. (2006). They indicated spectral flattening and turnover at ~ 100 MHz. However, it seems difficult to determine these accurately because the spot sizes are smaller than the VLA beam sizes at the above frequencies. The LOw Frequency ARray (LOFAR) (<http://www.lofar.org/>) and Square Kilometer Array (SKA) (<http://www.skatelescope.org/>) will, in the future, tell us the real turnover frequency with sufficiently high resolution.

6. *Thermal electron number density* n_{hs}^{T} . Here, we comment on the difficulty of constraining n_{hs}^{T} . We use the absence of bremsstrahlung emission. The X-ray observations for Cygnus A show the flux upper limit as $\sim 1 \times 10^{-13} \text{ erg s}^{-1} \text{ cm}^{-2}$ (e.g., Smith et al. 2002).

As already mentioned, the constraint from the intrinsic RM is not available, because plasma temperature is relativistic in the present work. Even worse, Cygnus A is known for its unusually large RM values; thus, it is not a good example from which to argue the intrinsic depolarization (Dreher et al. 1987; Garrington & Conway 1991). No evidence for intrinsic depolarization between 5 and 15 GHz is found, and the origin of the large RM is thought to be the external bow shock that surrounds the radio lobes (Dreher et al. 1987; Carilli et al. 1988). Hence, it is not appropriate to use the constraint from RM for Cygnus A.

6.2. Results

Below, we show the resultant allowed region of n_{hs} and n_p for cases (a), (b), (c), and (d).

6.2.1. Case (a)

Considering the uncertainties of $\Gamma_j \beta_j$ and β_{hs} , we examine two limiting cases, with $\Gamma_j \beta_j = 1$ and $\beta_{\text{hs}} = 0.01$ being a High- n case, and $\Gamma_j \beta_j = 30$ and $\beta_{\text{hs}} = 0.06$ being a Low- n case. For the High- n case, n_{hs} is about two orders of magnitude larger than that of the Low- n case.

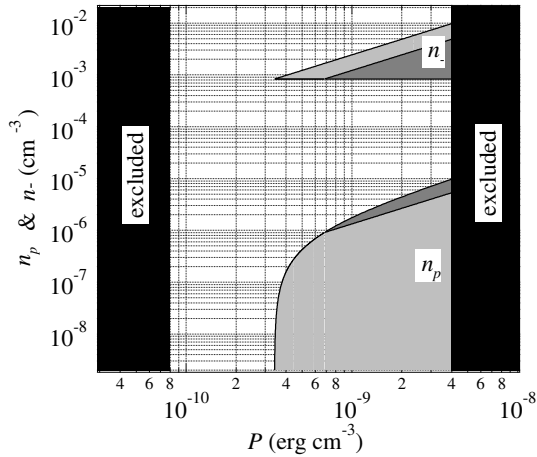


Figure 4. Allowed regions of n_- and n_+ for Cygnus A with $\Gamma_j \beta_j = 1$ and $\beta_{hs} = 0.01$ (we call this the High- n case). The region within $8 \times 10^{-11} \text{ erg cm}^{-3} \leq P \leq 4 \times 10^{-9} \text{ erg cm}^{-3}$ shown here is the one allowed for Cygnus A. As explained in Figure 3, the region in which $P_{\pm} > P_p$ holds is colored in light gray, while the region where $P_{\pm} > P_p$ is satisfied is colored in dark gray. It is found that e^{\pm} pairs always dominate in terms of number density but either a “pair-supported cocoon (i.e., $P_{\pm} > P_p$)” or a “proton-supported one (i.e., $P_{\pm} < P_p$)” is possible.

In Figure 4, we show the allowed regions of n_- and n_+ for the High- n case. First, we find that $n_- > n_+$ always holds, and this satisfies $\eta \sim 10^{-2}$ at $P = P_{\max}$. This implies that positron mixture is inevitable. In other words, $P_{1,\min}$ is much larger than P_{\max} obtained by the Cygnus A cocoon calorimetry. (If we are forced to make $P_{1,\min}$ smaller, then γ_{\min} becomes larger; such a case coincides with case (b).) The allowed regions of n_- and n_+ are further divided by two regions. The pair of light-gray regions show the one in which $P_{\pm} > P_p$ is satisfied. On the contrary, the pair of dark-gray regions display the one in which $P_{\pm} < P_p$ holds. Interestingly, we find that the regions of $P_p < P_{\pm}$ and $P_p > P_{\pm}$ are both wide in the range of allowed P . In the range of $P \sim (3\text{--}6) \times 10^{-10} \text{ erg cm}^{-3}$, the pair dominance $P_p < P_{\pm}$ alone is permitted in the High- n case.

Figure 5 displays the result for the Low- n case. Similar to the High- n case, $n_- > n_+$ always holds, and they satisfy $\eta \sim 10^{-1}$ at $P = P_{\max}$. Due to the decrease in $n_{-, \min}$, the number densities in allowed regions are about two orders of magnitude smaller than that for the High- n case shown in Figure 4. Correspondingly, $P_{0,\min}$, $P_{\text{eq},\min}$, and $P_{1,\min}$ decrease. Since $P_{\text{eq},\max} < P_{\max}$ is still satisfied, both of the regions with $P_p < P_{\pm}$ and that with $P_p > P_{\pm}$ are allowed in this case. In other words, the Low- n case also qualitatively draws the same conclusion with the High- n case. Quantitatively, the upper limit of n_+ becomes larger when $n_{-, \min}$ becomes smaller; correspondingly, the maximum η achieved at P_{\max} becomes larger by a factor of ~ 10 than that for the High- n case.

In summarizing case (a), we find that $\eta < 1$ always holds in the allowed range of P . In other words, this indicates the existence of e^{\pm} pairs in the cocoon. We find that (1) the e^{\pm} pair is dominant in terms of number density, and (2) both the “pair-supported cocoon (i.e., $P_{\pm} > P_p$)” and the “proton-supported one (i.e., $P_{\pm} < P_p$)” are allowed. The pair-supported cocoon is different from the previously suggested one in which protons are dynamically dominated (e.g., De Young 2006).

6.2.2. Case (b)

For Cygnus A, we face a difficulty of realizing one-temperature plasma. First, let us consider the case of the same

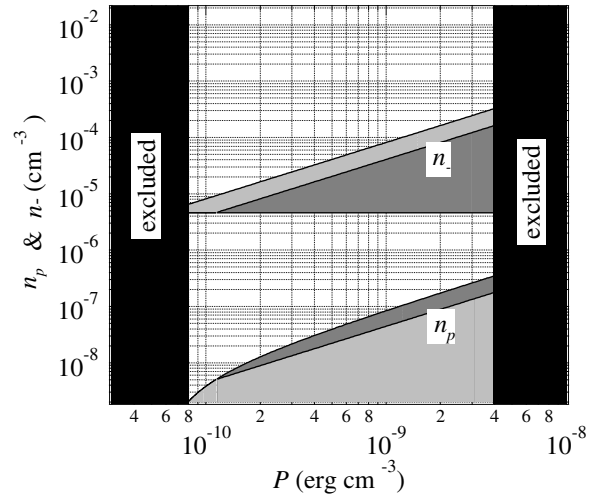


Figure 5. Same as Figure 4 but with $\Gamma_j = 30$ and $\beta_{hs} = 0.06$ (we call this the Low- n case). Although the allowed regions of n_- and n_+ are about two orders of magnitude smaller than the ones in Figure 4 (High- n case), the Low- n case draws the same conclusion as the High- n case.

$n_{-, \min}$ as in Figures 4 and 5. All of these thermal electrons should be heated to $kT_{\pm} \sim 10^4 m_e c^2$ and injected into the lobes in case (b). In the radio lobes, Yaji et al. (2010) evaluate the number density of non-thermal electrons as $\sim 10^{-7} \text{ cm}^{-3}$ at $\gamma_- \sim 10^4$. So, if we allow the existence of thermal plasma with the same $n_{-, \min}$ in Figures 4 and 5 but with $kT_{\pm} = kT_p \sim 10^4 m_e c^2$, a big thermal bump at $\sim 10^9 \text{ Hz}$ should appear. However, there is no such bump in the observed spectra of the radio lobes. Therefore, we can exclude the case of the same $n_{-, \min}$ with $kT_{\pm} = kT_p \sim 10^4 m_e c^2$.

Next, we consider smaller $n_{-, \min}$. Using the relation $n_{-, \min} \propto \gamma_{\text{hs}, \min}^{-1}$ in Equation (19), the increase in $\gamma_{\text{hs}, \min}$ leads to the decrease in $n_{-, \min}$ in Figures 4 and 5; basically, $\gamma_{\text{hs}, \min} \sim 10^4$ is required at the hot spot (e.g., Harris et al. 2000; Hardcastle et al. 2001; Blundell et al. 2006; Godfrey et al. 2009). However, in the case of Cygnus A, the model spectra of the hot spots with $\gamma_{\text{hs}, \min} \geq 2000$ conflict with the observed ones (KT04). Therefore, case (b) is not likely for Cygnus A.

6.2.3. Case (c)

Let us consider the case of dominant non-thermal pressures and a separate acceleration of electrons and protons with a steep power-law spectrum. This is almost identical to case (a). A slight difference between this case and case (a) is the evaluation of $n_{-, \min}$. Since non-thermal pairs are dominated in this case, the allowed region would be limited around $n_- \approx n_{-, \min}$ in Figures 4 and 5.

6.2.4. Case (d)

Let us consider case (d). The factor $A_{\pm} = (\gamma_{\pm, \text{crit}}/\gamma_{\pm, \min})^{-s+2}$ in Equation (14) is the only element to change the result from case (a). Since $\gamma_{\text{crit}, \pm} \sim m_p/m_e$ is suggested by Stawarz et al. (2007), we can estimate A_{\pm} as $A_{\pm} \approx 14(\Gamma_j/10)^{0.5}$ for $s_{e,1} = 1.5$. Therefore, a difference between this case and case (a) is the larger P_{\pm} by a factor of A_{\pm} . Although the spectral break may be suggested from radio observations for case (d), n_-^{NT} is dominated by electrons at a break energy $\gamma_{\text{crit}, \pm} m_e c^2$, and proton energies are not entirely transported to electrons. Therefore, results of case (d) are expected to be intermediate between cases (a) and (b).

7. SUMMARY AND DISCUSSIONS

In this work, we propose a new method for testing plasma composition of AGN jets using cocoon dynamics. In particular, we properly evaluate partial pressures of protons and e^\pm pairs. The point of the method is that n_p and P_p can be constrained by considering the global conservations of kinetic energy, mass, and momentum of shocked plasma in the cocoon. Regarding particle distribution functions in the cocoon, it is hard to determine them uniquely because of the sparseness of observational data. Therefore, we examine four typical cases in this work. Cases (a), (b), (c) and (d), respectively, present two-temperature thermal plasma, one-temperature thermal plasma, non-thermal plasma with their spectral indices harder than two, and non-thermal plasma with a broken power-law electron spectrum.

The three significant advantages of the present work compared with previous work are summarized as follows:

1. P estimate is based on global cocoon dynamics. Since it is beaming-independent calorimetry of the true amount of energy released by the jet, the estimate of P from cocoon dynamics has fewer uncertainties compared with blazar studies.
2. We focus on powerful FR II sources. Relativistic hydrodynamic simulations tell us that FR II sources have less entrainment phenomena than FR I sources. Therefore, FR IIs are better for testing genuine plasma composition of AGN jets.
3. We properly deal with the partial pressure of thermal electrons/positrons P_\pm^T . Although P_\pm^T is a critically important finite quantity, most prior efforts assume $P_\pm^T = 0$ merely for simplicity.

Applying the method to the best-studied FR II source Cygnus A, we draw the following conclusions, which primarily indicate the existence of numerous e^\pm pairs in the cocoon of Cygnus A:

1. Cases (a), (c), and (d), in which the average energy of electrons and positrons is significantly lower than that of protons ($\eta < 10^{-1}$ for Low- n case; $\eta < 10^{-2}$ for High- n case), are allowed without violating the observational constraints. The results in cases (a) and (c) are almost the same, except that the lowest energy electrons are thermal ones and non-thermal ones for cases (a) and (c), respectively. Cases (a) and (d) show similar results but for a P_\pm in case (d) larger by a factor of ~ 14 than the one in case (a).
2. We can rule out case (b), in which electrons and positrons are heated to the proton temperature of $\sim 10^4 m_p c^2$, because there is no thermal bump due to the hot thermal plasma.
3. For cases (a), (c), and (d), we find that the number density of e^\pm is larger than in any allowed P , and the obtained n_+ is always more than 10 times larger than n_p . We conclude that pure e/p plasma is excluded and e^\pm -proton mixture composition is achieved in the Cygnus A jet. Therefore, further studies of the e^\pm pair loading problem extending previous ones (e.g., Blandford & Levinson 1995; Li & Liang 1996; Thompson 1997; Beloborodov 1999; Yamasaki et al. 1999) will be important, and the study of its bulk acceleration of e^\pm outflow (Iwamoto & Takahara 2002, 2004; Asano & Takahara 2007, 2009) will also be highly motivated.
4. We find that both e/p plasma and e^\pm pair pressure supported scenarios are permitted within the limits of current

observational constraints. We quantitatively show the allowed regions of $P_p > P_\pm$ and $P_p < P_\pm$ by our new method (see Figures 4 and 5).

Last, we add a brief comment on P_p^{NT} . Recently, Atayan & Dermer (2008) suggested the possibility of a secondary emission induced by high-energy protons at Cygnus A. The luminosity of the secondary emission depends on P_p^{NT} . If the emission is detected in the future, it will provide a new direct constraint on P_p^{NT} . It could also give a new constraint on cosmic-ray propagations influenced by the galactic magnetic field (Dermer et al. 2009).

We thank the referee for useful suggestions for major improvement of the original manuscript. We also thank H. Ito for helpful discussions. This work is supported in part by Ministry of Education, Culture, Sports, Science, and Technology (MEXT) Research Activity Start-up 2284007 (N.K.).

REFERENCES

- Achterberg, A., Gallant, Y. A., Kirk, J. G., & Guthmann, A. W. 2001, *MNRAS*, **328**, 393
- Amato, E., & Arons, J. 2006, *ApJ*, **653**, 325
- Arnaud, K. A., Fabian, A. C., Eales, S. A., Jones, C., & Forman, W. 1984, *MNRAS*, **211**, 981
- Asano, K., & Takahara, F. 2007, *ApJ*, **655**, 762
- Asano, K., & Takahara, F. 2009, *ApJ*, **690**, L81
- Atayan, A., & Dermer, C. D. 2008, *ApJ*, **687**, L75
- Bach, U., Kadler, M., Krichbaum, T. P., et al. 2003, in Proc. Second ENIGMA Meeting, ed. C. M. Raiteri & M. Villata (Porto Venere, Italy: ENIGMA), 216
- Bach, U., Krichbaum, T. P., Alef, W., Witzel, A., & Zensus, J. A. 2002, in Proc. 6th European VLBI Network Symposium, ed. E. Ros, R. W. Porcas, A. P. Lobanov, & J. A. Zensus (Bonn: MPIfR), 155
- Bednarz, J., & Ostrowski, M. 1998, *Phys. Rev. Lett.*, **80**, 3911
- Begelman, M. C., Blandford, R. D., & Rees, M. J. 1984, *Rev. Mod. Phys.*, **56**, 255
- Begelman, M. C., & Cioffi, D. F. 1989, *ApJ*, **345**, L21
- Beloborodov, A. M. 1999, *MNRAS*, **305**, 181
- Bicknell, G. V. 1984, *ApJ*, **286**, 68
- Birzan, L., McNamara, B. R., Nulsen, P. E. J., Carilli, C. L., & Wise, M. W. 2008, *ApJ*, **686**, 859
- Blandford, R. D., & Levinson, A. 1995, *ApJ*, **441**, 79
- Blandford, R. D., & Znajek, R. L. 1977, *MNRAS*, **179**, 433
- Blundell, K. M., Fabian, A. C., Crawford, C. S., Erlund, M. C., & Celotti, A. 2006, *ApJ*, **644**, L13
- Carilli, C. L., & Barthel, P. D. 1996, *A&AR*, **7**, 1
- Carilli, C. L., Perley, R. A., & Dreher, J. H. 1988, *ApJ*, **334**, L73
- Carilli, C. L., Perley, R. A., Dreher, J. W., & Leahy, J. P. 1991, *ApJ*, **383**, 554
- Carilli, C. L., Perley, R., Harris, D. E., & Barthel, P. D. 1998, *Phys. Plasmas*, **5**, 1981
- Cavagnolo, K. W., McNamara, B. R., Nulsen, P. E. J., et al. 2010, *ApJ*, **720**, 1066
- Croston, J. H., Hardcastle, M. J., Harris, D. E., et al. 2005, *ApJ*, **626**, 733
- Dermer, C. D., Razaque, S., Finke, J. D., & Atayan, A. 2009, *New J. Phys.*, **11**, 065016
- De Young, D. S. 1993, *ApJ*, **405**, L13
- De Young, D. S. 2006, *ApJ*, **648**, 200
- Dreher, J. W., Carilli, C. L., & Perley, R. A. 1987, *ApJ*, **316**, 611
- Dunn, R. J. H., Fabian, A. C., & Taylor, G. B. 2005, *MNRAS*, **364**, 1343
- Fabian, A. C., Celotti, A., Blundell, K. M., Kassim, N. E., & Perley, R. A. 2002, *MNRAS*, **331**, 369
- Garrington, S. T., & Conway, R. G. 1991, *MNRAS*, **250**, 198
- Georganopoulos, M., Kazanas, D., Perlman, E., & Stecker, F. W. 2005, *ApJ*, **625**, 656
- Ghisellini, G., & Tavecchio, F. 2010, *MNRAS*, **409**, L79
- Godfrey, L. E. H., Bicknell, G. V., Lovell, J. E. J., et al. 2009, *ApJ*, **695**, 707
- Hardcastle, M. J., Birkinshaw, M., & Worrall, D. M. 2001, *MNRAS*, **323**, L17
- Hardcastle, M. J., & Croston, J. H. 2010, *MNRAS*, **404**, 2018
- Harris, D. E., & Krawczynski, H. 2006, *ARA&A*, **44**, 463
- Harris, D. E., Nulsen, P. E. J., Ponman, T. J., et al. 2000, *ApJ*, **530**, L81
- Hirotoni, K. 2005, *ApJ*, **619**, 73
- Hirotoni, K., Iguchi, S., Kimura, M., & Wajima, K. 1999, *PASJ*, **51**, 263

- Hirotani, K., Iguchi, S., Kimura, M., & Wajima, K. 2000, *ApJ*, **545**, 100
- Homan, D. C., Lister, M. L., Aller, H. D., Aller, M. F., & Wardle, J. F. C. 2009, *ApJ*, **696**, 328
- Hoshino, M., Arons, J., Gallant, Y. A., & Langdon, A. B. 1992, *ApJ*, **390**, 454
- Huang, L., & Shcherbakov, R. V. 2011, *MNRAS*, **416**, 2574
- Ichimarū, S. (ed.) 1973, *Basic Principles of Plasma Physics, A Statistical Approach*, (Reading, MA: Benjamin), 324
- Isobe, N., Makishima, K., Tashiro, M., & Hong, S. 2005, *ApJ*, **632**, 781
- Isobe, N., Tashiro, M., Makishima, K., et al. 2002, *ApJ*, **580**, L111
- Ito, H., Kino, M., Kawakatu, N., Isobe, N., & Yamada, S. 2008, *ApJ*, **685**, 828 (I08)
- Iwamoto, S., & Takahara, F. 2002, *ApJ*, **565**, 163
- Iwamoto, S., & Takahara, F. 2004, *ApJ*, **601**, 78
- Kataoka, J., Madejski, G., Sikora, M., et al. 2008, *ApJ*, **672**, 787
- Kawakatu, N., & Kino, M. 2006, *MNRAS*, **370**, 1513
- Kellermann, K. I., Lister, M. L., Homan, D. C., et al. 2004, *ApJ*, **609**, 539
- Kellermann, K. I., & Pauliny-Toth, I. I. K. 1981, *ARA&A*, **19**, 373
- Kino, M., & Kawakatu, N. 2005, *MNRAS*, **364**, 659
- Kino, M., Kawakatu, N., & Ito, H. 2007, *MNRAS*, **376**, 1630
- Kino, M., & Takahara, F. 2004, *MNRAS*, **349**, 336 (KT04)
- Kino, M., & Takahara, F. 2008, *MNRAS*, **383**, 713
- Kirk, J. G., Guthmann, A. W., Gallant, Y. A., & Achterberg, A. 2000, *ApJ*, **542**, 235
- Komissarov, S. S., Barkov, M. V., Vlahakis, N., & Königl, A. 2007, *MNRAS*, **380**, 51
- Krichbaum, T. P., Alef, W., Witzel, A., et al. 1998, *A&A*, **329**, 873
- Lazio, T. J. W., Cohen, A. S., Kassim, N. E., et al. 2006, *ApJ*, **642**, L33
- Li, H., & Liang, E. P. 1996, *ApJ*, **458**, 514
- Lister, M. L., Aller, H. D., Aller, M. F., et al. 2009, *AJ*, **137**, 3718
- Lister, M. L., Tingay, S. J., Murphy, D. W., et al. 2001, *ApJ*, **554**, 948
- Machalski, J., Jamrozny, M., & Konar, C. 2010, *A&A*, **510**, A84
- Melrose, D. B. 1997, *J. Plasma Phys.*, **58**, 735
- Miley, G. 1980, *ARA&A*, **18**, 165
- Mizuta, A., Yamada, S., & Takabe, H. 2004, *ApJ*, **606**, 804
- McKinney, J. C. 2006, *MNRAS*, **368**, 1561
- McKinney, J. C., Tchekhovskoy, A., & Blandford, R. D. 2012, arXiv:1201.4163
- Mehta, K. T., Georganopoulos, M., Perlman, E. S., Padgett, C. A., & Chartas, G. 2009, *ApJ*, **690**, 1706
- Perley, R. A., Dreher, J. W., & Cowan, J. J. 1984, *ApJ*, **285**, L35
- Perlman, E. S., Georganopoulos, M., May, E. M., & Kazanas, D. 2010, *ApJ*, **708**, 1
- Perucho, M., & Martí, J. M. 2007, *MNRAS*, **382**, 526
- Quataert, E., & Gruzinov, A. 2000, *ApJ*, **545**, 842
- Rachen, J. P., & Biermann, P. L. 1993, *A&A*, **272**, 161
- Rafferty, D. A., McNamara, B. R., Nulsen, P. E. J., & Wise, M. W. 2006, *ApJ*, **652**, 216
- Rawlings, S., & Saunders, R. 1991, *Nature*, **349**, 138
- Reynolds, C. S., Fabian, A. C., Celotti, A., & Rees, M. J. 1996, *MNRAS*, **283**, 873
- Rossi, P., Mignone, A., Bodo, G., Massaglia, S., & Ferrari, A. 2008, *A&A*, **488**, 795
- Ruszkowski, M., & Begelman, M. C. 2002, *ApJ*, **573**, 485
- Scheck, L., Aloy, M. A., Martí, J. M., Gómez, J. L., & Müller, E. 2002, *MNRAS*, **331**, 615
- Scheuer, P. A. G. 1995, *MNRAS*, **277**, 331
- Sikora, M., & Madejski, G. 2000, *ApJ*, **534**, 109
- Sironi, L., & Spitkovsky, A. 2011, *ApJ*, **726**, 75
- Smith, D. A., Wilson, A. S., Arnaud, K. A., Terashima, Y., & Young, A. J. 2002, *ApJ*, **565**, 195
- Spitkovsky, A. 2008, *ApJ*, **682**, L5
- Stawarz, L., Cheung, C. C., Harris, D. E., & Ostrowski, M. 2007, *ApJ*, **662**, 213
- Steenbrugge, K. C., Blundell, K. M., & Duffy, P. 2008, *MNRAS*, **388**, 1465
- Steenbrugge, K. C., Heywood, I., & Blundell, K. M. 2010, *MNRAS*, **401**, 67
- Svensson, R. 1982, *ApJ*, **258**, 335
- Takahara, F. 1990, *Prog. Theor. Phys.*, **83**, 1071
- Tashiro, M., Kaneda, H., Makishima, K., et al. 1998, *ApJ*, **499**, 713
- Tashiro, M. S., Isobe, N., Seta, H., Matsuta, K., & Yaji, Y. 2009, *PASJ*, **61**, 327
- Thompson, C. 1997, in *Proc. Int. Conf., Relativistic Jets in AGNs*, ed. M. Ostrowski, M. Sikora, G. Madejski, & M. Begelman (Krakow: Poligrafia ITS), 63
- Uchiyama, Y., Urry, C. M., Van Duynne, J., et al. 2005, *ApJ*, **631**, L113
- Wardle, J. F. C., Homan, D. C., Ojha, R., & Roberts, D. H. 1998, *Nature*, **395**, 457
- Watanabe, S., Sato, R., Takahashi, T., et al. 2009, *ApJ*, **694**, 294
- Wilson, A. S., Smith, D. A., & Young, A. J. 2006, *ApJ*, **644**, L9
- Wilson, A. S., Young, A. J., & Shopbell, P. L. 2000, *ApJ*, **544**, L27
- Yaji, Y., Tashiro, M., Isobe, N., et al. 2010, *ApJ*, **714**, 37
- Yamasaki, T., Takahara, F., & Kusunose, M. 1999, *ApJ*, **523**, L21